ChemCatChem

Research Article
doi.org/10.1002/cctc.202400749

Chemistry Europe
European Chemical Societies Publishing

www.chemcatchem.org

Nitrogen, Fluorine, and Phosphorus Tri-Doped Porous Carbon with High Electrical Conductivity as an Excellent Metal-Free Electrocatalyst for Oxygen Reduction Reaction

Ryuji Takada,*[a] Kotaro Narimatsu,[a] Yurika Taniguchi,[a] Xinran Yang,[a] Koji Miyake,*[a, b] Yoshiaki Uchida,[a] and Norikazu Nishiyama[a, b]

Today's oxygen reduction reaction (ORR) depends on the precious metal Pt-based catalysts, limiting the large commercialization of promising energy conversion technologies such as proton exchange membrane fuel cells (PEMFCs) and metal-air batteries. Therefore, the rational design of low-cost and highly efficient electrocatalysts for ORR is strongly desired. Herein, we report a porous carbon doped with nitrogen, fluorine, and phosphorus (N, F, P tri-doped carbon) prepared via only a heating process using low-cost glycine, ammonium fluoride, and phytic acid as precursors. X-ray photoelectron spectroscopy (XPS) analysis revealed the existence of pyridinic-N and the co-existence of graphitic-N and oxidized graphitic-P, which can be active sites, with semi-ionic C–F bonds highly boosting ORR activity. Remarkably, the resultant N, F, P tri-doped carbon exhibited outstanding activity for the ORR with an onset potential comparable to that of commercial 20 wt% Pt/C catalyst, the half-wave potential superior to that of the Pt/C catalyst, and the electron transfer number close to 4.

Introduction

With the increasing demand for clean energy, renewable energy conversion systems have attracted interest in addressing the accelerating fossil fuel consumption and serious environmental issues.[1–3] Among the energy conversion systems, proton exchange membrane fuel cells (PEMFCs) and metal-air batteries have been recognized as promising alternatives of existing systems depending on fossil fuels due to their environmental friendliness and high theoretical energy density.[4–7] Unfortunately, the sluggish kinetics of the oxygen reduction reaction (ORR) with multi-electron transfer at cathodes decrease the energy conversion efficiency of the above-mentioned devices.[8–10] Until now, Pt-based catalysts have been widely used as commercial electrocatalysts for ORR. However, the scarcity, high cost, and low durability of Pt hinder the large-scale application of Pt-based catalysts.[11–14] Therefore, great efforts have been devoted to exploring cost-effective, stable, and highly active electrocatalysts with non-precious metals.

Recently, metal-free carbon catalysts doped with heteroatoms, such as N,[15,16] P,[17] B,[18] and S,[19] have been extensively explored and are regarded as one of the most favorable candidates for ORR because of their abundance, low cost, and high stability. In addition, metal-free heteroatom doped carbons show high-tolerance to CH_3OH and avoid metal particle agglomeration and dissolution in electrolytes.[20,21] The ORR activity heteroatom doped carbons originate from the difference of electronegativity between C atom and heteroatoms, leading to charge transfer. The density functional theoretical (DFT) calculations demonstrate that introducing heteroatoms results in a different spin density and charge density redistribution on C atoms adjacent to the heteroatoms, which facilitate the O_2 adsorption.[22–26] Among them, heteroatom co-doping is an effective way to tune the catalytic activity by the synergistic effect.[27–32] Furthermore, the specific surface area and pore structure of carbon catalysts perform a good function in improving ORR activity.[33,34] Recently, we have synthesized N, P co-doped carbon catalysts with precisely controlled pore structures from bio-based raw materials via combined processes of pyrolysis and CO_2 activation. The N, P co-doped carbon catalysts showed high catalytic performance on the ORR.[35] Like our previous research, various heteroatom co-doped carbons with high performance have been reported, however, there is still room for improvement in the catalytic performance of the catalysts comparable to that Pt-based catalysts on ORR. However, there is still room for improvement in the catalytic performance of the catalysts on ORR. Nowadays, introducing F atoms is considered as an effective way to boost ORR activity. F doping bring about the maximum charge delocalization on the adjacent carbon atoms due to their higher high electronegativity, which intensively improves the O_2 adsorption.[36,37] C–F bonds are classified into ionic, semi-ionic, and covalent C–F bonds in their nature. The formation of covalent C–F bonds

[a] R. Takada, K. Narimatsu, Y. Taniguchi, X. Yang, K. Miyake, Y. Uchida, N. Nishiyama
Division of Chemical Engineering, Graduate School of Engineering Science, Osaka University, 1-3 Machikaneyama, Toyonaka, Osaka 560-8531, Japan
E-mail: r.takada@cheng.es.osaka-u.ac.jp
kojimiyake@cheng.es.osaka-u.ac.jp

[b] K. Miyake, N. Nishiyama
Innovative Catalysis Science Division, Institute for Open and Transdisciplinary Research Initiatives (ICS-OTRI), Osaka University, Suita 565-0871, Japan

Supporting information for this article is available on the WWW under https://doi.org/10.1002/cctc.202400749

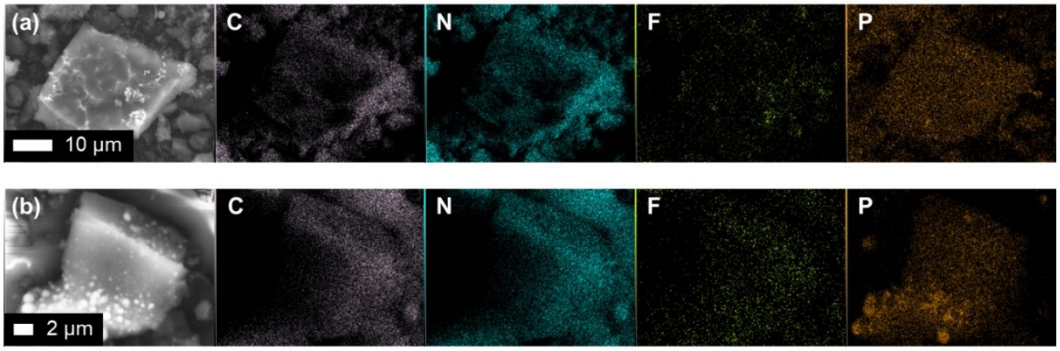

Figure 1. Elemental mapping images of (a) CNFP and (b) CNFP-act.

reduces the electrical conductivity because covalent C–F bonds break the π-conjugated bonds in graphene.[38] On the other hand, F atoms semi-ionic bonded to C atoms act as electron acceptors and promote the C–C bond polarization, which enhances the electrical conductivity.[39,40]

Herein, we present a facile synthesis of N, F, P tri-doped carbons as a metal-free electrocatalyst for the ORR by a pyrolysis of glycine, ammonium fluoride, and phytic acid as precursors. We introduced P atoms because we revealed that oxidized graphitic-P plays an important role in the synergistic effects of N and P atoms in our previous work. F doping was conducted to gain the high electrical conductivity. In addition to carbonization, CO_2 activation was performed to tune the pore structure. The obtained catalysts were characterized systematically, and then electrochemical measurements were performed to investigate the catalytic activity for the ORR.

Results and Discussion

First, the electrocatalytic activities of N, F, P tri-doped carbon (CNFP) carbonized at 900, 1000, and 1100 °C for ORR were evaluated using linear sweep voltammetry (LSV) in 0.1 M KOH to determine the optimal carbonization temperature. These catalysts are denoted as CNFP-*T* (*T* is carbonization temperature). As shown in Figure S1a, CNFP-1000 exhibited the highest catalytic activity; thus, 1000 °C was the optimal carbonization temperature. The ORR activities of CNFP mixed from different raw material composition carbonized at 1000 °C were also evaluated to determine the optimal N, F, and P composition. These catalysts are denoted as CNFP(*x*) ($x = 0.5$, 1, 2; *x* is relative mass ratio to glycine or phytic acid). As displayed in Figure S1b, CNFP(1) exhibited the highest ORR activity; thus raw materials composition of CNFP(1) was the optimal value (hereinafter, CNFP-1000 or CNFP(1) is called CNFP). The yield of CNFP from raw materials is 4.83 %. The CNFP was activated with CO_2, and the obtained catalyst was denoted as CNFP-act. The final yield of CNFP-act based on raw materials was 2.80 %. CNF and CNP are N, F and N, P co-doped carbon, respectively.

The morphologies of the synthesized catalysts were investigated by transmission electron microscopy (TEM). As displayed in Figure S2, the layer structures and aggregated carbon particles with random diameters were observed for all the catalysts. Scanning electron microscopy-energy-dispersive X-ray spectroscopy (SEM-EDX) and CHN elemental analysis were conducted to confirm the successful synthesis of N, F, and P tri-doped carbon. Figure 1 shows the elemental mapping images obtained via SEM-EDX, suggesting that N, F, and P atoms were uniformly distributed. The relative C, N, F, P, O, and H contents were measured by the combination of CHN elemental analysis and EDX analysis (Table 1). The relative C content of CNFP-act was lower than that of CNFP, which is attributed to the influence of CO_2 activation. The CO_2 activation process can be described by the following equation:[41,42]

$$C_n + CO_2 = C_{n-1} + 2CO$$

At high temperatures, some of the C atoms in the catalysts are gasified to CO by CO_2, leading to the generation of pore structures. In addition, the relative P content of CNFP-act was larger than that of CNFP, suggesting that the P atoms did not disappear during CO_2 activation. The main changes of the relative N and F contents were not observed after CO_2 activation. The catalysts were further investigated by X-ray diffraction (XRD). As shown in Figure S3, two broad diffraction peaks centered at ~25° and ~44° were found in all the catalysts, corresponding to the (002) and (100) planes of carbon, respectively. It suggests that the crystalline nature of all the catalysts.[43,44] From the above, the successful synthesis of N, F, and P tri-doped carbons was confirmed.

The N_2 adsorption measurements were performed to determine the specific surface areas and pore properties of CNFP catalysts. The N_2 adsorption isotherms and pore size distributions of CNF, CNP, CNFP, and CNFP-act are shown in

Table 1. The C, N, F, P, O, and H contents of each catalyst.

Catalysts	C [wt%]	N [wt%]	F [wt%]	P [wt%]	O [wt%]	H [wt%]
CNF	65.43	4.81	2.58	–	26.11	1.07
CNP	72.30	3.40	–	11.66	11.56	1.08
CNFP	77.13	2.72	0.36	6.20	12.85	0.74
CNFP-act	68.30	3.12	0.34	9.68	18.26	0.30

Figure 2, and the BET surface areas and pore volumes of each pore region are listed in Table S1. Micropore size distributions (Figure 2b) and mesopore size distribution (Figure 2c) were investigated using MP-plot and BJH methods, respectively. All the catalysts except for CNF exhibited larger specific surface area and pore volume. In particular, as shown in Figure 2b, a significant difference in micropores was observed, implying that phytic acid as a P precursor functioned as an activator, such as H_3PO_4 activation.[45,46] The specific surface area of CNFP was larger than that of CNP because of the etching by a part of NH_4F.[47,48] Furthermore, the BET surface areas and pore volumes of CNFP-act increased due to CO_2 activation, and the increase in mesopores was significant (Figure 2c). A larger BET surface areas and pore volumes are beneficial for ORR. The micropores exposed the active sites, expecting to enhance the onset potential. Mesopores promote the O_2 diffusion in the pore, expecting to improve the current.[49,50] Especially, the micropores and mesopores with the diameters close to those of micropores may enhance the onset potential.[35]

The X-ray photoelectron spectroscopy (XPS) measurements were carried out to reveal the chemical composition and bonding state of the catalyst surfaces. As shown in Figure 3a, the high-resolution N 1s spectrum can be fitted into two peaks centered at 398.5 eV and 401.0 eV, corresponding to pyridinic-N and graphitic-N, respectively.[51–53] The P 2p spectrum (Figure 3c) was deconvoluted three peaks at 132.2 eV, 133.4 eV, and 136.4 eV, attributable to graphitic-P, oxidized graphitic-P, and phosphate oxide, respectively.[54,55] Notably, the rate of pyridinic-N for CNFP-act is higher than that for CNFP and graphitic-P vanished in CNFP-act. This is because of the increase of edge sites by CO_2 activation. Graphitic-N and graphitic-P exposed outer catalyst surface and became pyridinic-N and oxidized graphitic-P combined with oxygen, respectively. It has been proven that pyridinic-N contributes to the improvement of catalytic activity for ORR. We have revealed that co-existence of graphitic-N and oxidized graphitic-P forms the appropriate active sites for ORR. The F 1s spectrum (Figure 3b) is divided into ionic (684.6 eV) and semi-ionic (688.3 eV) C–F bonds.[56–58] The covalent C–F bonds leading to low conductivity were absent in all the catalysts. The polarization effect of semi-ionic C–F bonds is higher than that of ionic C–F bonds. The existence of semi-ionic C–F bonds further enhance the catalytic performance.[59,60]

The electrocatalytic activities of CNF, CNP, CNFP, and CNFP-act in ORR were performed using LSV in 0.1 M KOH. For comparison, the same measurements were performed using a commercial 20 wt% Pt/C catalyst (Figure 4a and Table 2). CNFP showed a better onset potential than CNF, suggesting that N, P co-doping brings about active sites, namely the co-existence of graphitic-N and oxidized graphitic-P. The larger micropore volumes also contributed to improving the onset potentials of the CNP and CNFP. CNFP presented a better catalytic activity than CNP, indicating that the C–C bond polarization with semi-ionic C–F bonds enhance the O_2 adsorption and electrical

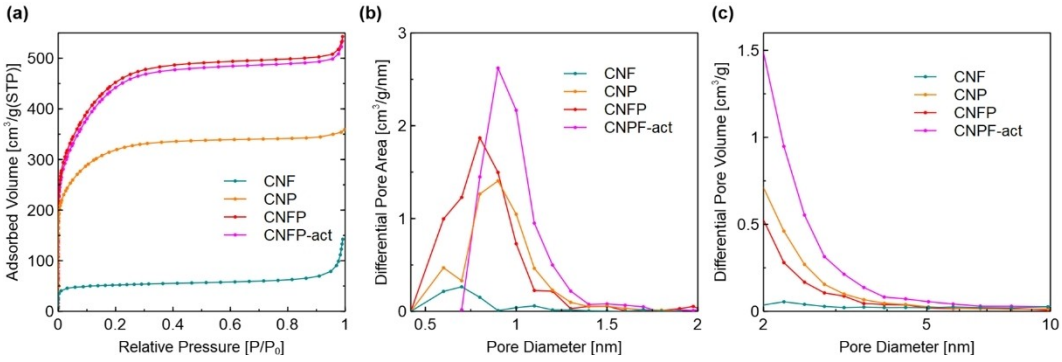

Figure 2. (a) N_2 adsorption isotherms, (b) micropore size distributions, and (c) mesopore size distributions of CNF, CNP, CNFP, and CNFP-act.

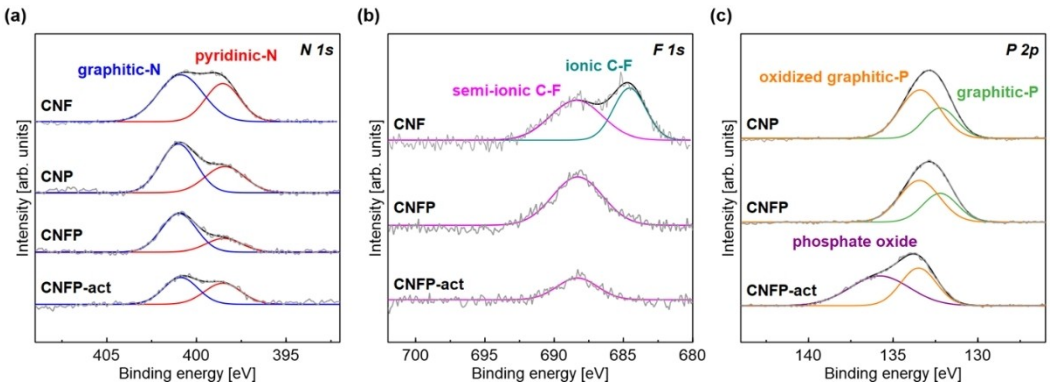

Figure 3. (a) N 1s, (b) F 1s, and (c) P 2p XPS spectrum of each catalyst.

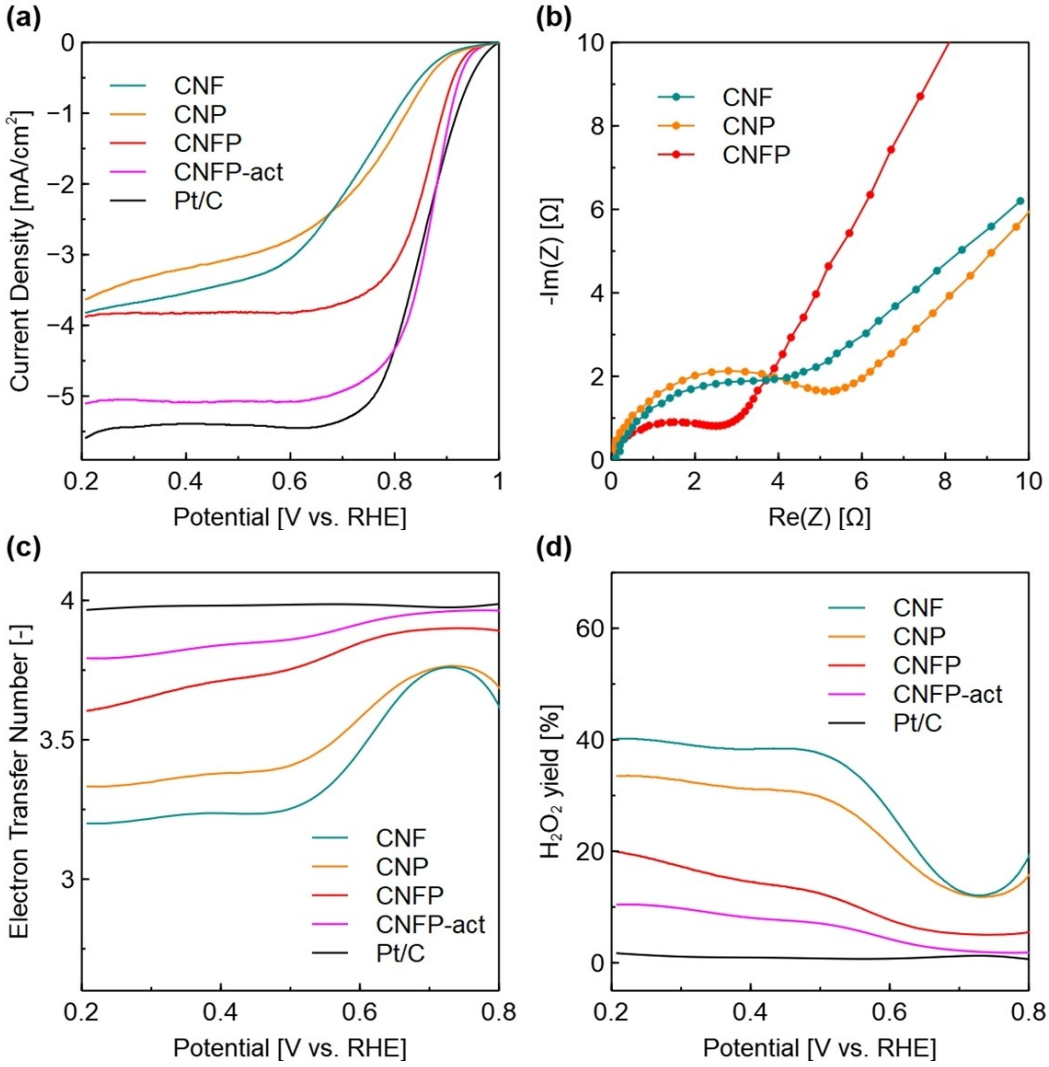

Figure 4. (a) LSV voltammograms, (b) electrochemical impedance spectrum, (c) number of transferred electrons, and (d) H_2O_2 yield for each catalyst recorded with stirring at 1600 rpm in an O_2-saturated 0.1 M KOH solution at a scan rate of 5 mV s^{-1}.

Table 2. Onset and half-wave potentials and limiting current density of each catalyst.

Catalysts	Onset potential [V vs. RHE]	Half-wave potential [V vs. RHE]	Limiting current density [mA cm^{-2}]
CNF	0.873	0.745	−3.82
CNP	0.892	0.787	−3.63
CNFP	0.924	0.860	−3.88
CNFP-act	0.931	0.867	−5.10
Pt/C	0.948	0.856	−5.56

conductivity, which fasten their subsequent O_2 reduction.[61,62] The electrochemical impedance spectrum demonstrated that the resistances of CNF and CNFP were lower than that of CNP (Figure 4b). The superior performance of CNFP is attributed to the favorable active sites resulting from the synergistic effects of N, P co-doping and the improvement of O_2 adsorption and the promotion of the ORR by F doping. Furthermore, CNFP-act displayed an excellent ORR activity, with an onset of 0.931 V vs. RHE and a half-wave potential of 0.867 V vs. RHE, respectively. The larger mesopore volume of CNFP-act than that of CNFP enhanced O_2 diffusion, leading to the further improvements of half-wave potential and current density. The onset potential of CNFP-act was comparable to that of Pt/C (0.948 V vs. RHE) and the half-wave potential of CNFP-act exceeded that of Pt/C catalyst (0.856 V vs. RHE). As listed in Table S2, the onset and half-wave potentials of CNFP-act were superior to those of heteroatom-doped metal-free catalysts reported in previous studies.

The electron transfer number and hydrogen peroxide yield of each catalyst were measured to further investigate the excellent ORR activity. As presented in Figure 4c, the electron transfer number of CNFP-act was 3.80–3.96 in the oxygen diffusion-controlled region (0.2–0.8 V), which demonstrate the promotion of four-electron ORR pathway. The exposed rich active sites with high electrical conductivity due to CO_2 activation and semi-ionic C–F bonds contribute to efficient O_2

reduction. The H_2O_2 yield of CNFP-act was below approximately 10% in the oxygen diffusion-controlled region (0.2–0.8 V).

The durability and crossover effect are other important factors for ORR electrocatalysts.[63,64] Thus, the long-term durability and methanol tolerance of CNFP-act and Pt/C catalysts were performed using chronoamperometry (Figure S4). CNFP-act showed a good stability with a decrease to 91.3% after 7200 s. In addition, CNFP-act retains the performance after adding methanol, whereas an obvious drop of current was observed for Pt/C catalyst. The N, P, F tri-doped carbon possesses not only excellent catalytic activity but also high durability and methanol tolerance.

To gain the insight into ORR activity in acidic media, LSV measurements for CNFP-act and Pt/C were conducted in 0.5 M H_2SO_4 (Figure S5). CNFP-act also showed high activity even in acidic media with an onset potential of 0.760 V vs. RHE, which is close to that of Pt/C (0.799 V vs. RHE). Furthermore, the H_2O_2 yield of CNFP-act was approximately 0%in the oxygen diffusion-controlled region (0.2–0.6 V vs. RHE). The performance of CNFP-act in acidic media is comparable and superior to that of other metal-free catalysts reported in the literature (Table S3).

Conclusions

In summary, we proposed the simple method to synthesize N, F, P tri-doped carbons as a metal-free electrocatalyst for ORR by only pyrolysis processes of inexpensive raw materials with high porosity and controlled heteroatoms. The optimized catalyst, CNFP-act, exhibited a superior catalytic activity for ORR to other metal-free heteroatom-doped carbon catalysts reported in the literature, with the onset potential of 0.931 V vs. RHE, half-wave potential of 0.867 V vs. RHE, and electron transfer number close to 4, which are comparable and even overcome those of commercial 20 wt% Pt/C catalyst. The remarkable performance of CNFP-act is attributed to its porous structure and preferable active sites, the dopant of pyridinic N or co-dopant of graphitic-N and oxidized graphitic-P, with the high conductivity boosted by semi-ionic C–F bonds. CNFP-act also showed long-term stability, methanol tolerance, and high ORR activity even in acidic media; thus, this work provides not only rational design of efficient ORR catalysts but also great opportunities for practical application. Future work should investigate the fuel cell performance because this work is limited to the discussion of the catalytic activity using a single cell.

Experimental Section

Materials

Glycine, aqueous solutions of 50 wt% phytic acid, ammonium fluoride, and Nafion (5 wt%) were purchased from FUJIFILM Wako Pure Chemical (Osaka, Japan); the Pt/C catalyst (20 wt%) was purchased from Sigma-Aldrich (St. Louis, MO, USA); N_2 gas (purity 99.99%) and CO_2 gas (purity 99.5%) was purchased from Iwatani (Osaka, Japan). All the materials were used as received without further purification.

Synthesis of CNFP

An overview of prepared samples in this work is summarized in Scheme 1. In a typical synthesis, Glycine, phytic acid, and ammonium fluoride at an equivalent mass ratio were dissolved in deionized water. The solution was placed in a ceramic boat and dried at 90 °C, and the dried solid material was carbonized for 3 h at 1000 °C under an N_2 atmosphere. The obtained carbon catalyst was denoted as CNFP. CNF was obtained using glycine and ammonium fluoride as precursors and CNP was obtained using glycine and phytic acid as precursors by the same carbonization process. Furthermore, CNFP was activated with CO_2 for 4 h at 825 °C and was named CNFP-act. All the heating processes were performed at a rate of 5 °C $min^{<M-1>1}$.

Furthermore, CNP (0.1 g) was activated with CO_2 for a certain period of time at a certain temperature. The heating was performed at a rate of 5 °C min^{-1}.

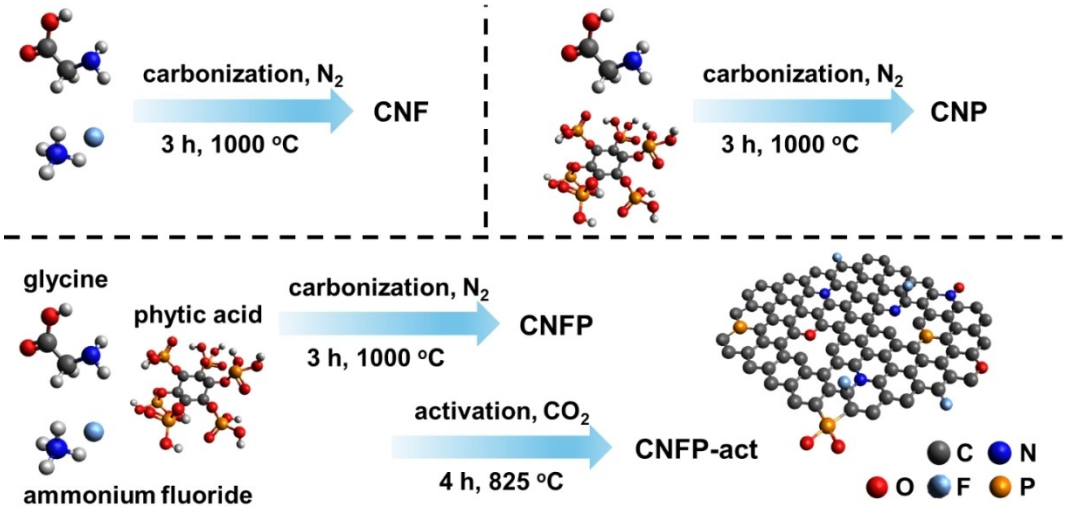

Scheme 1. Schematic of the synthesis of N, F, and P tri-doped carbon. Carbon, nitrogen, oxygen, fluorine, and phosphorus atoms are shown in gray, blue, red, light blue, and orange, respectively.

Characterizations

Transmission Electron Microscopy (TEM) and Scanning Electron Microscopy-Energy-Dispersive X-ray spectroscopy (SEM-EDX) were respectively performed using an H800 (Hitachi, Tokyo, Japan) and a JCM-7000 (JEOL, Tokyo, Japan). X-ray diffraction (XRD) was carried out on a PANalytical X'Pert-MDR diffractometer using Cu Kα radiation. X-ray photoelectron spectroscopy (XPS) analysis was performed using a Kratos Ultra 2 (Shimadzu, Kyoto, Japan), and the N_2 adsorption isotherms were measured at −196.15 °C using a BELSORP MINI X (Microtrac MRB, Osaka, Japan). Accordingly, the specific surface areas and pore volumes and size distributions were determined using the Brunauer–Emmett–Teller (BET), MicroPore analysis (MP)-Plot, and Barrett–Joyner–Halenda (BJH) methods. Organic elemental analysis was conducted using FlashEA (Thermo Fisher Scientific, Waltham, MA, USA).

Preparation of the Working Electrodes

Nafion (5 wt% in alcohol and water), isopropanol, and water were mixed to prepare the catalyst dispersion solution at a volume ratio of 1:1:8. This solution (1 mL) was added to the catalyst (8.8 mg) and ultrasonicated at least 30 minutes to prepare the catalyst ink. Subsequently, the ink (8 μL) was dropped onto the glassy carbon of a Rotating Ring-Disk Electrode (RRDE) with a diameter of 4 mm and an area of 0.1256 cm^2, yielding a mass loading of 0.56 mg cm^{-2}.

Electrochemical Measurements

A three-electrode configuration was used for the electrochemical measurements. The RRDE electrode with the glassy carbon disk (4.0 mm in diameter) and a Pt ring (inner and outer diameters of 5.0 and 7.0 mm, respectively), an Hg/Hg_2Cl_2 (saturated KCl solution) electrode, and a graphite rod were used as the working, reference, and counter electrodes, respectively. The potentials reported herein are relative to the Reversible Hydrogen Electrode (RHE) and based on the following equations:

$$E_{RHE} = E_{Hg/Hg_2Cl_2} + 1.0083 \ (\text{in 0.1 M KOH}) \quad (1)$$

$$E_{RHE} = E_{Hg/Hg_2Cl_2} + 0.2444 \ (\text{in 0.5 M } H_2SO_4) \quad (2)$$

Linear Sweep Voltammetry (LSV) was performed in O_2-saturated 0.1 M KOH and 0.5 M H_2SO_4 solution with a scan rate of 5 mV s^{-1}, and the potential was applied from 1.2 to 0.2 V for ORR. Prior to LSV measurements, O_2 was bubbled in electrolyte for 30 minutes. During the tests O_2 was bubbled continuously. The ring potential was maintained at 1.5 V vs. RHE to calculate the number of transferred electrons and rate of H_2O_2 production during LSV using the following equations:

$$n = (4 \times I_d)/(I_d + I_r/N) \quad (3)$$

$$H_2O_2\,\% = 200 \times (I_r/N)/(I_d + I_r/N) \quad (4)$$

where I_d is the disk current obtained using the disk electrode, I_r is the oxidation current obtained using the ring electrode, and N is the collection efficiency of the ring, which was experimentally determined as 0.37.

Electrochemical impedance spectroscopy (EIS) was also tested in O_2-saturated 0.1 M KOH at 0.6 V vs. RHE with the amplitude of 10 mV and the frequency range of 10^6 Hz–0.1 Hz.

Supporting Information

Supporting Information is available from the Wiley Online Library or from the author.

Acknowledgements

The study was partially conducted using a facility at the Research Center for Ultra-High Voltage Electron Microscopy, Osaka University, Suita, Japan.

Conflict of Interests

The authors declare no conflict of interest.

Data Availability Statement

The data that support the findings of this study are available from the corresponding author upon reasonable request.

Keywords: heteroatom doped carbon · oxygen reduction reaction (ORR) · metal-free catalyst · CO_2 activation · semi-ionic C–F bond

[1] B. Dunn, H. Kamath, J.-M. Tarascon, *Science* **2011**, *334*, 928.
[2] F. T. Wagner, B. Lakshmanan, M. F. Mathias, *J. Phys. Chem. Lett.* **2010**, *1*, 2204.
[3] P. C. K. Vesborg, T. F. Jaramillo, *RSC Adv.* **2012**, *2*, 7933.
[4] B. C. H. Steele, A. Heinzel, *Nature* **2001**, *414*, 345.
[5] F. Cheng, J. Chen, *Chem. Soc. Rev.* **2012**, *41*, 2172.
[6] M. K. Debe, *Nature* **2012**, *486*, 43.
[7] B. Li, Y. Chen, X. Ge, J. Chai, X. Zhang, T. S. A. Hor, G. Du, Z. Liu, H. Zhang, Y. Zong, *Nanoscale* **2016**, *8*, 5067.
[8] L. Li, L. Hu, J. Li, Z. Wei, *Nano Res.* **2015**, *8*, 418.
[9] J. Suntivich, H. A. Gasteiger, N. Yabuuchi, H. Nakanishi, J. B. Goodenough, Y. Shao-Horn, *Nature Chem.* **2011**, *3*, 546.
[10] E. M. Erickson, M. S. Thorum, R. Vasić, N. S. Marinković, A. I. Frenkel, A. A. Gewirth, R. G. Nuzzo, *J. Am. Chem. Soc.* **2012**, *134*, 197.
[11] S. Zhang, Y. Cai, H. He, Y. Zhang, R. Liu, H. Cao, M. Wang, J. Liu, G. Zhang, Y. Li, H. Liu, B. Li, *J. Mater. Chem. A* **2016**, *4*, 4738.
[12] G.-L. Li, X. Wang, F. Deng, Z.-F. Lu, C. Hao, S. Wang, G. Sun, *Catal. Sci. Technol.* **2023**, doi:10.1039/D3CY00498H.
[13] J. Zhang, Z. Zhao, Z. Xia, L. Dai, *Nature Nanotech.* **2015**, *10*, 444.
[14] C. Ehlert, A. Piras, J. Schleicher, G. Gryn'ova, *J. Phys. Chem. Lett.* **2023**, *14*, 476.
[15] H. Jiang, J. Gu, X. Zheng, M. Liu, X. Qiu, L. Wang, W. Li, Z. Chen, X. Ji, J. Li, *Energy Environ. Sci.* **2019**, *12*, 322.
[16] Q. Lv, N. Wang, W. Si, Z. Hou, X. Li, X. Wang, F. Zhao, Z. Yang, Y. Zhang, C. Huang, *Appl. Catal., B* **2020**, *261*, 118234.
[17] H. Zhao, Z.-P. Hu, Y.-P. Zhu, L. Ge, Z.-Y. Yuan, *Chin. J. Catal.* **2019**, *40*, 1366.
[18] L. Yang, S. Jiang, Y. Zhao, L. Zhu, S. Chen, X. Wang, Q. Wu, J. Ma, Y. Ma, Z. Hu, *Angew. Chem. Int. Ed.* **2011**, *50*, 7132.
[19] I.-Y. Jeon, S. Zhang, L. Zhang, H.-J. Choi, J.-M. Seo, Z. Xia, L. Dai, J.-B. Baek, *Adv. Mater.* **2013**, *25*, 6138.
[20] A. Srinu, S. G. Peera, V. Parthiban, B. Bhuvaneshwari, A. K. Sahu, *ChemistrySelect* **2018**, *3*, 690.
[21] S. Akula, A. K. Sahu, *ACS Appl. Mater. Interfaces* **2020**, *12*, 11438.
[22] R. Li, Z. Wei, X. Gou, *ACS Catal.* **2015**, *5*, 4133.
[23] J. Y. Cheon, J. H. Kim, J. H. Kim, K. C. Goddeti, J. Y. Park, S. H. Joo, *J. Am. Chem. Soc.* **2014**, *136*, 8875.

[24] Y. Wang, L. Tao, Z. Xiao, R. Chen, Z. Jiang, S. Wang, *Adv. Funct. Mater.* **2018**, *28*, 1705356.
[25] G.-L. Chai, K. Qiu, M. Qiao, M.-M. Titirici, C. Shang, Z. Guo, *Energy Environ. Sci.* **2017**, *10*, 1186.
[26] S. G. Peera, R. Koutavarapu, S. Akula, A. Asokan, P. Moni, M. Selvaraj, J. Balamurugan, S. O. Kim, C. Liu, A. K. Sahu, *Energy Fuels* **2021**, *35*, 11761.
[27] Y. Chang, C. Yuan, C. Liu, J. Mao, Y. Li, H. Wu, Y. Wu, Y. Xu, B. Zeng, L. Dai, *J. Power Sources* **2017**, *365*, 354.
[28] J. Yu, C. Wang, W. Yuan, Y. Shen, A. Xie, *Chem. Eur. J.* **2019**, *25*, 2877.
[29] Z. Liu, M. Wang, X. Luo, S. Li, S. Li, Q. Zhou, W. Xu, R. Wu, *Appl. Surf. Sci.* **2021**, *544*, 148912.
[30] Y. Zan, Z. Zhang, H. Liu, M. Dou, F. Wang, *J. Mater. Chem. A* **2017**, *5*, 24329.
[31] Y. Shu, Y. Takada, R. Takada, Y. Taniguchi, K. Miyake, Y. Uchida, C. Y. Kong, N. Nishiyama, *Adv. Mater. Interfaces* **2023**, *10*, 2300088.
[32] J. Li, Y. Zhang, X. Zhang, J. Huang, J. Han, Z. Zhang, X. Han, P. Xu, B. Song, *ACS Appl. Mater. Interfaces* **2017**, *9*, 398.
[33] L. Chen, Y. Zhang, Z. Liu, L. Hou, X. Liu, *Energy Adv.* **2024**, doi: 10.1039/D3YA00493G.
[34] H. Wang, J. Ding, J. Zhang, C. Wang, W. Yang, H. Ren, A. Kong, *RSC Adv.* **2016**, *6*, 79928.
[35] R. Takada, Y. Shu, Y. Taniguchi, X. Yang, K. Miyake, Y. Uchida, N. Nishiyama, *Carbon* **2024**, *218*, 118719.
[36] S. Akula, B. Balasubramaniam, P. Varathan, A. K. Sahu, *ACS Appl. Energy Mater.* **2019**, *2*, 3253.
[37] S. Akula, V. Parthiban, S. G. Peera, B. P. Singh, S. R. Dhakate, A. K. Sahu, *J. Electrochem. Soc.* **2017**, *164*, F568.
[38] T. Jin, J. Chen, C. Wang, Y. Qian, L. Lu, *J Mater Sci* **2020**, *55*, 12103.
[39] G. Panomsuwan, N. Saito, T. Ishizaki, *J. Mater. Chem. A* **2015**, *3*, 9972.
[40] M. Li, Q. Ye, S. Hou, J. Yang, B. Chi, Y. Deng, X. Tian, *J. Mater. Chem. A* **2023**, *11*, 8730.
[41] T. Mori, S. Iwamura, I. Ogino, S. R. Mukai, *J. Porous Mater.* **2017**, *24*, 1497.
[42] X. Lan, X. Jiang, Y. Song, X. Jing, X. Xing, *Green Process. Synth.* **2019**, *8*, 837.
[43] Z. Zhou, T. Liu, A. U. Khan, G. Liu, *Mol. Syst. Des. Eng.* **2020**, *5*, 153.
[44] M. Etesami, R. Khezri, S. Rezaei Motlagh, M. Gopalakrishnan, M. Thanh Nguyen, T. Yonezawa, S. Wannapaiboon, K. Nootong, A. Somwangthanaroj, S. Kheawhom, *ChemCatChem* **2023**, *15*, e202300724.
[45] O. Oginni, K. Singh, G. Oporto, B. Dawson-Andoh, L. McDonald, E. Sabolsky, *Bioresour. Technol. Rep.* **2019**, *8*, 100307.
[46] Y. Li, X. Zhang, R. Yang, G. Li, C. Hu, *RSC Adv.* **2015**, *5*, 32626.
[47] B. Qu, X. Yu, Y. Chen, C. Zhu, C. Li, Z. Yin, X. Zhang, *ACS Appl. Mater. Interfaces* **2015**, *7*, 14170.
[48] L. Huang, K. Zhong, Y. Wu, Y. Wu, X. Liu, L. Huang, J. Yan, H. Zhang, *Carbon* **2023**, *207*, 86.
[49] Y. Liu, K. Li, B. Ge, L. Pu, Z. Liu, *Electrochim. Acta* **2016**, *214*, 110.
[50] S. Wang, Y. Chen, Y. Zhao, G. Wei, D. Li, X. Liu, *J Mater Sci* **2022**, *57*, 19431.
[51] Y. Lv, L. Yang, D. Cao, *ACS Appl. Mater. Interfaces* **2017**, *9*, 32859.
[52] W. Chen, L. Xu, Y. Tian, H. Li, K. Wang, *Carbon* **2018**, *137*, 458.
[53] J. Quílez-Bermejo, M. Melle-Franco, E. San-Fabián, E. Morallón, D. Cazorla-Amorós, *J. Mater. Chem. A* **2019**, *7*, 24239.
[54] A. R. MacIntosh, G. Jiang, P. Zamani, Z. Song, A. Riese, K. J. Harris, X. Fu, Z. Chen, X. Sun, G. R. Goward, *J. Phys. Chem. C* **2018**, *122*, 6593.
[55] L. Dong, C. Hu, X. Huang, N. Chen, L. Qu, *Chem. Asian J.* **2015**, *10*, 2609.
[56] P. F. Fulvio, S. S. Brown, J. Adcock, R. T. Mayes, B. Guo, X.-G. Sun, S. M. Mahurin, G. M. Veith, S. Dai, *Chem. Mater.* **2011**, *23*, 4420.
[57] J. Zhang, L. Dai, *Angew. Chem. Int. Ed.* **2016**, *55*, 13296.
[58] S. G. Peera, A. K. Sahu, A. Arunchander, S. D. Bhat, J. Karthikeyan, P. Murugan, *Carbon* **2015**, *93*, 130.
[59] S. Akula, P. Varathan, A. Kesh, K. Tammeveski, S. G. Peera, S. K. Panda, B. Balasubramaniam, A. K. Sahu, *Int. J. Hydrog. Energy* **2022**, *47*, 20617.
[60] S. Akula, A. K. Sahu, *J. Electrochem. Soc.* **2019**, *166*, F93.
[61] S. Akula, S. G. Peera, A. K. Sahu, *J. Electrochem. Soc.* **2019**, *166*, F897.
[62] S. Akula, P. Varathan, R. S. Menon, A. K. Sahu, *Sustainable Energy Fuels* **2021**, *5*, 886.
[63] B. Choi, W.-H. Nam, D. Y. Chung, I.-S. Park, S. J. Yoo, J. C. Song, Y.-E. Sung, *Electrochim. Acta* **2015**, *164*, 235.
[64] M. Asteazaran, G. Cespedes, S. Bengió, M. S. Moreno, W. E. Triaca, A. M. Castro Luna, *J. Appl. Electrochem.* **2015**, *45*, 1187.

Manuscript received: April 24, 2024
Revised manuscript received: June 19, 2024
Accepted manuscript online: July 7, 2024
Version of record online: ■■, ■■

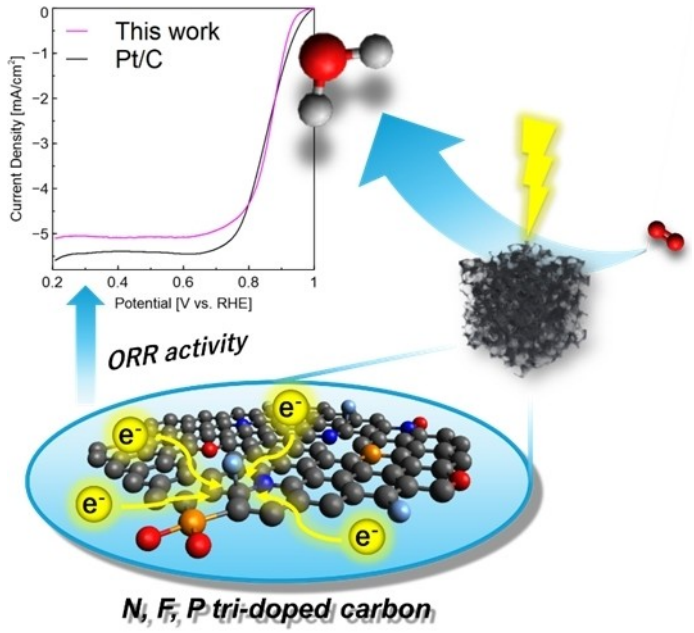

R. Takada, K. Narimatsu, Y. Taniguchi, X. Yang, K. Miyake*, Y. Uchida, N. Nishiyama*

1 – 8

Nitrogen, Fluorine, and Phosphorus Tri-Doped Porous Carbon with High Electrical Conductivity as an Excellent Metal-Free Electrocatalyst for Oxygen Reduction Reaction

N, F, P tri-doped porous carbon catalysts exhibit excellent ORR activity in alkaline and acidic media. XPS measurements reveals the preferable active sites with high conductivity by semi-ionic C–F bonds. This work provides not only rational design of efficient ORR catalysts but also great opportunities for practical application.